SEISMIC SAFETY EVALUATION OF HIGH CONCRETE DAMS PART II: EARTHQUAKE BEHAVIOR OF ARCH DAMS: CASE STUDY

Zhang Chuhan[1], Jin Feng[1], Pan Jianwen[1], Long Yuchuan[1,2]

[1]State Key Laboratory Hydroscience and Engineering, Tsinghua University, Beijing, China
[2]Dept. of Civil Engineering, Chongqing University, Chongqing, China
Email: zch-dhh@tsinghua.edu.cn

ABSTRACT:

A case study on the Dagangshan arch dam to resist the design earthquake using state-of-the-art techniques is performed considering different input mechanisms, nonlinearity of contraction joint opening, damage fracture behavior and strengthening of the dam and then some concluding remarks are given.

KEYWORDS: arch dams, earthquake input mechanisms, contraction joint, damage-cracking, strengthening

1. INTRODUCTION

1.1. General Description

The Dagangshan arch dam with a height of 210 meters and a dam crest arc length of 609.8 meters is under construction on the Dadu River of Southwest China. The thicknesses of the crown cantilever are 52 meters at the bottom and 10 meters at the crest. The arc length-height ratio and thickness-height ratio are 2.90 and 0.248 respectively. The total number of contraction joints in the dam is twenty-eight. The normal depth of reservoir water is 205 meters and the lowest reservoir depth in operation is 195 meters, and the depth of silt sedimentation during operation is 125 meters. The dam is located in an extremely strong earthquake region with the design PGA=0.557g. Safety evaluation of the dam subjected to the design earthquake is a crucial factor for the project. The linear elastic and nonlinear dynamic behavior analyses including contraction joint opening and damage-cracking of concrete are performed to study the response of the dam under the design earthquake. In terms of earthquake input mechanism and foundation modeling, both the massless foundation and mass-viscous-spring boundary model are used for comparison.

1.2. Material Parameters, Loading Conditions and Design Earthquake

The values of material parameters adopted in the analysis are obtained from material tests carried out by the Chengdu Hydroelectric Investigation & Design Institute. The dynamic elastic modulus of concrete and rock is multiplied by 1.3 of their static counterparts respectively. The parameters are summarized in Table 4.1. The material damping is considered via Rayleigh damping assumption in the analyses.

The normal static loads including the dam gravity, reservoir water, silt pressures, and design temperature loads are imposed first. The dynamic loads include earthquakes in the three directions and the hydrodynamic

pressures. The design peak ground accelerations are 0.557g in the stream and cross-stream directions, and 0.371g in the vertical direction. The response spectra of the design earthquake are shown in Figure 1, which are stipulated in the specification DL-5073-2000. The hydrodynamic interaction is modeled via the added mass assumption, based on finite element method with incompressible reservoir fluid. Finite element analysis provides the fundamental periods for full and lowest reservoir elevations are 0.6s and 0.56s respectively.

Table 4.1 Material properties of the Dagangshan arch dam

	Concrete	Rock
Elastic modulus (MPa)	3.12×10^4	1.885×10^4
Poisson ratio ν	0.17	0.258
Unit weight (kN/m^3)	24.0	26.5

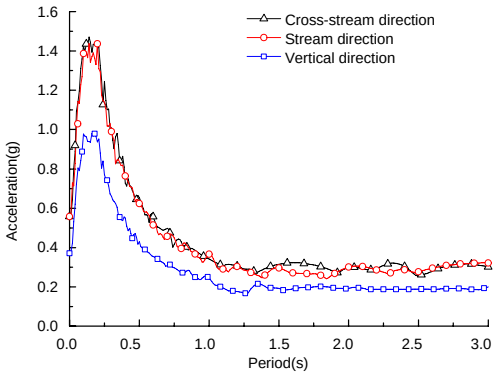

Figure 1 Design acceleration response spectra

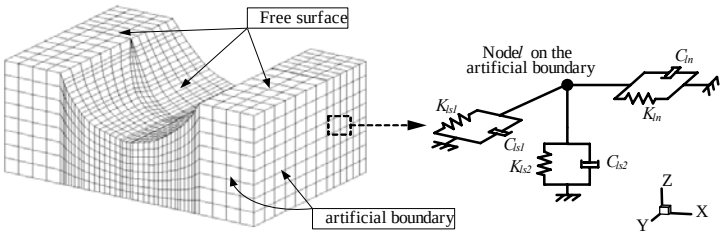

Figure 2 Sketch of the viscous-spring boundary

2. COMPUTATIONAL RESULTS

2.1. Comparison Study on Canyon Response by Different Foundation Input Models

Since the viscous-spring boundary is efficient and convenient to incorporate with current FE code and has sufficient accuracy without much increasing computational effort, the model is used herein.

In the viscous-spring boundary input model, three pairs of dashpots and springs are installed in each node of artificial boundaries as shown in Figure 2.

The parameters of springs and dashpots of node l on the artificial boundary are given as follows

$$K_{ln} = a\cdot\frac{\lambda+2G}{r};C_{ln}=b\rho c_p \qquad (4.1)$$

$$K_{ls} = a\cdot\frac{G}{r};C_{ls}=b\rho c_s \qquad (4.2)$$

where subscript l is the node number on the artificial boundary; n and s refer to the normal and tangential direction of the boundary plane; K is the elastic stiffness of the spring; C is the viscous damping; λ and G are the Lame's constants; c_p and c_s denote the P and S-wave velocity respectively; ρ is the mass density; r is the distance from the wave source to the node l; a and b are modification coefficients, which may be determined

from parameter analysis.

Herein, earthquake motions are transformed into nodal dynamic loads and exerted directly on the artificial boundaries. To satisfy the force equilibrium conditions at the artificial boundaries, the equivalent traction exerted on the node *l* can be expressed as

$$f_l(t) = K_l u_0(x_l, y_l, z_l, t) + C_l \dot{u}_0(x_l, y_l, z_l, t) + \sigma_0(x_l, y_l, z_l, t) \qquad (4.3)$$

where, $u_0(x_l, y_l, z_l, t)$ is the displacement of the free field at node *l*; $\dot{u}_0(x_l, y_l, z_l, t)$ and $\sigma_0(x_l, y_l, z_l, t)$ are determined by $u_0(x_l, y_l, z_l, t)$; K_l and C_l denote the elastic stiffness of the spring and viscous damping of the dashpot at node *l* respectively. The first two terms on the right-hand side of equation（4.3）are respectively the added elastic and damping forces to counteract those exerted on the artificial boundary by springs and dashpots. Also, these springs and dashpots may be viewed as radiation energy absorbers for scattering waves reflected by the canyon. The third term, σ_0, represents tractions at the truncated boundaries due to the input waves which usually take one half values of the free-field due to 1-D deconvolution. Therefore, this model may be categorized as a deconvolution method.

To study the influence of the different earthquake input mechanisms on the canyon response, several dynamic analyses of the Dagangshan canyon without the dam are performed. With verification of accuracy by different mesh size of elements and different range of foundation cut, the canyon cut profiles with viscous-spring boundary shown in Figure 3 is adequate to represent the canyon cut in a half space. The details of accuracy verification may be found elsewhere [56].

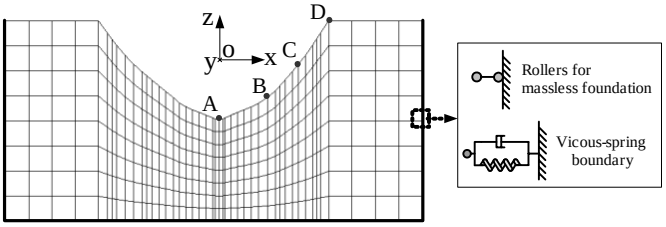

Figure 3 Canyon profile and FE mesh

Figure 4 shows the distribution of Peak Ground Acceleration (PGA) along the canyon surface and the corresponding acceleration response spectra respectively. The PGAs along the canyon surface in massless foundation model are completely uniform and exactly the same as the input. For mass-viscous-spring boundary model, the PGA distributes a spatially non-uniform pattern along the canyon surface due to wave scattering effects. In the two horizontal directions, compared with the massless foundation model, the most PGAs of the canyon surface are significantly reduced except the canyon terrace Point D, where a much larger PGA is observed. However, it is noteworthy that the amplification effects at Point D are simply due to the assumption of the leveling surface of the terrace while it seldom exists in a practical canyon for dam projects. Therefore, effects of different slopes of the canyon above the dam crest on the response of crest abutment need further study. In the vertical direction, larger PGAs are found in the viscous-spring boundary model. Furthermore, it can be found that smaller values of acceleration response spectra, especially in the period range of 0.5-1.0s, are vividly seen implying a significant reduction of the arch dam response can be expected.

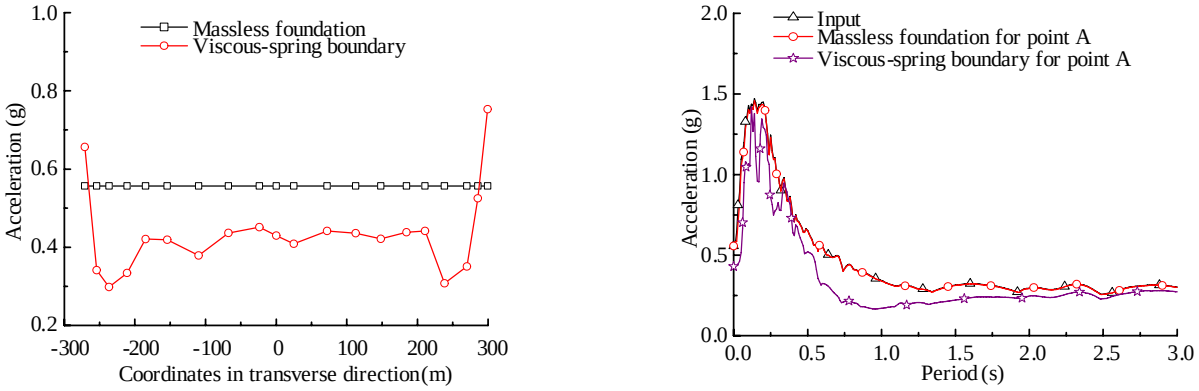

(a) Cross-stream direction

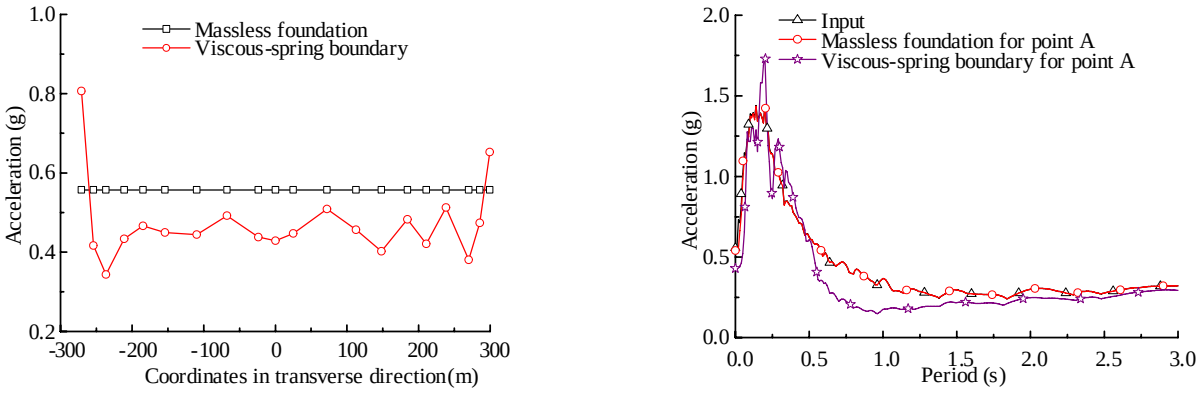

(b) Stream direction

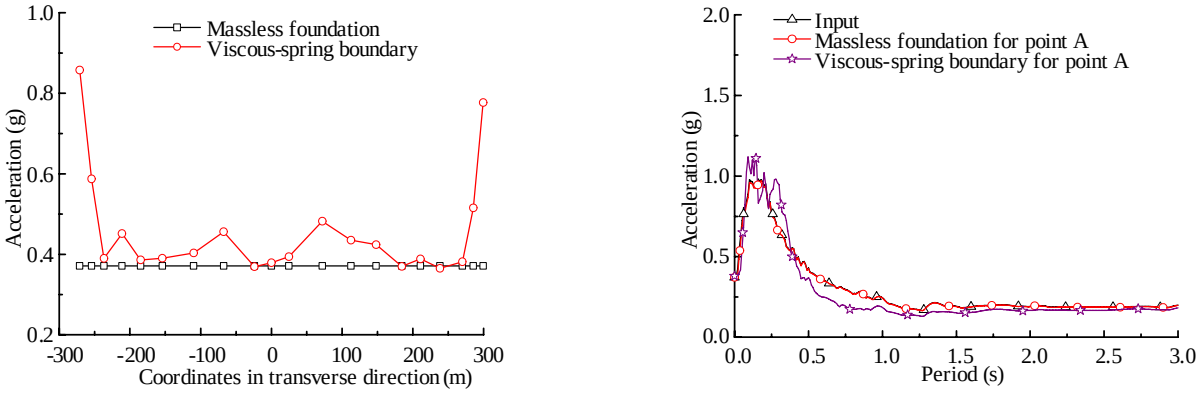

(c) Vertical direction

Figure 4 Acceleration response of the canyon

2.2. Comparison Study on Linear Elastic Response of the Dam by Different Foundation Input Models

Finite element discretization for arch dam-foundation system with contraction joints layout is shown in Figure 5. When the linear elastic dynamic analysis is performed, the joints are removed from the FE model and the whole dam-foundation system returns to a continuum.

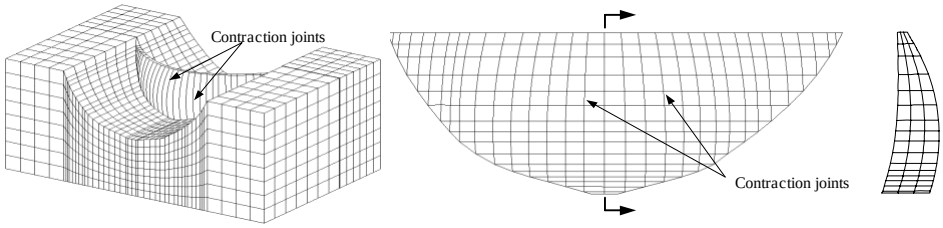

Figure 5 FE discretization of Dagangshan arch dam

Three cases of seismic analyses of the Dagangshan arch dam are performed including linear analysis using massless foundation input model with 5% and 10% damping ratio respectively, and viscous-spring boundary input model with 5% damping ratio for dam.

The distributions of maximum principal stresses on dam surfaces and crest displacements are shown in Figures 6 and 7. Significant difference in stress and displacement response between the two models is evident when both use 5% damping ratios. However, when increasing the damping ratio to 10% for massless foundation input model, the response of the maximum tensile stresses and displacements are similar to those obtained from the viscous-spring boundary input model except that the location of the maximum stress point of the upstream face shifts from the left to right quarter region while retaining a similar value of maximum stress.

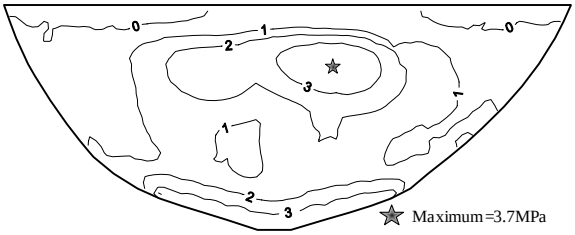

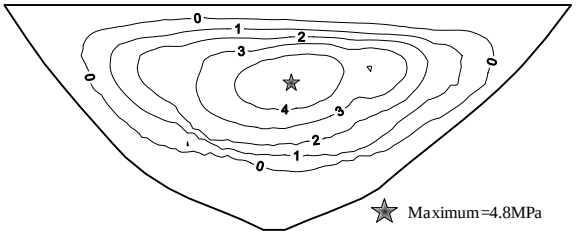

(I) Upstream (II) Downstream

(a) Massless foundation input model with 5% damping ratio for dam

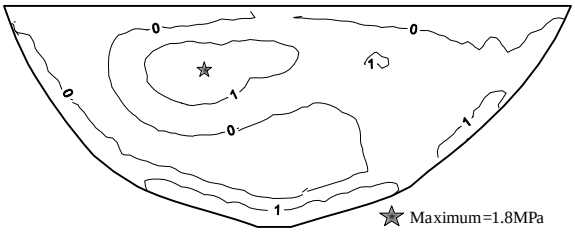

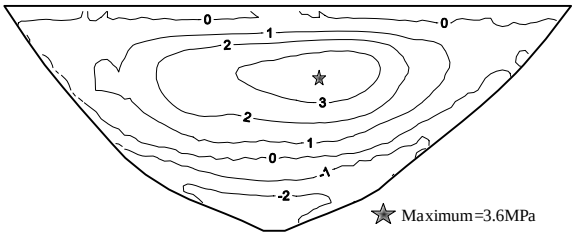

(I) Upstream (II) Downstream

(b) Massless foundation input model with 10% damping ratio for dam

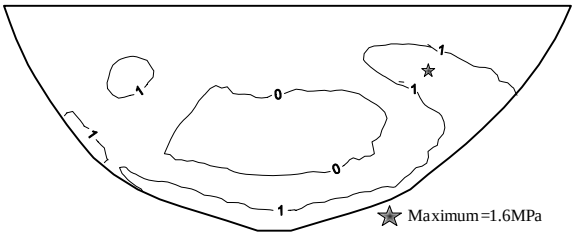

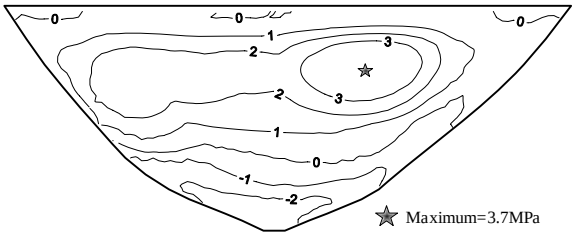

(I) Upstream (II) Downstream

(c) viscous-spring boundary model with 5% damping ratio for dam

Figure 6 Maximum principal stresses from linear elastic analysis

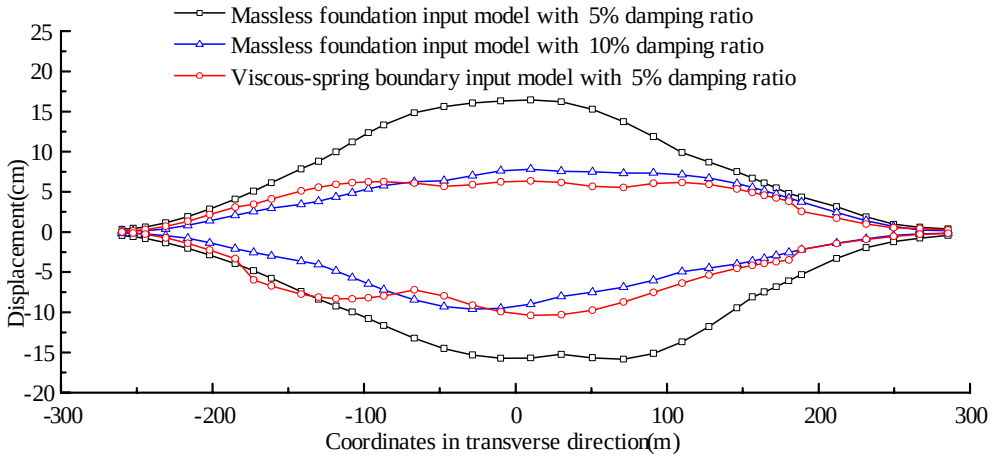

Figure 7 Maximum displacements along the dam crest from linear elastic analysis

It is concluded that the massless foundation input model overestimates the dam response because of ignoring the radiation effects; in this case, the reduction may reach 25-40% in terms of peak tensile stresses and crest displacements. These results strongly support conclusions of earlier research by Chopra *et al* [4], Dominguez *et al* [3] and Zhang *et al* [2,8]. Interestingly, in the Dagangshan case, if the damping ratio for the massless foundation is increased to 10%, the response will be approximately comparable to considering the effects of radiation damping due to the infinite foundation. Conceptually, for other dam canyons, this increased damping value may change depending on frequency closeness between the dam-canyon system and the input motions, as well as the flexibility of the foundation.

2.3. Comparison Study on Contraction Joint Opening of the Dam by Different Foundation Input Models

In nonlinear seismic analysis, the contact boundary model [22] with tangential springs is introduced to simulate the behavior of contraction joints. All the twenty-eight joints are simulated in the study. Herein, the same three cases as linear elastic analysis are performed.

Comparisons of stress distributions are shown in Figure 8. The maximum tensile stresses from all three analyses are 10% to 25% larger than the corresponding linear elastic cases due to the release of the arch action. The maximum tensile stresses from massless foundation with 10% damping ratio are still higher than the results from the viscous-spring boundary model with 5% damping ratio.

The maximum stream displacements along the dam crest are shown in Figure 9. The displacements in the analysis with 10% damping ratio are close (toward upstream) or larger (toward downstream) compared with that of the viscous-spring boundary model with 5% damping ratio.

The maximum opening of contraction joints is shown in Figure 10. The peak opening is 16.7mm and occurs at the right joint in the massless foundation model with 5% damping ratio, while in the other two cases the peak openings of 13.8mm and 9.6mm occur at the left joint respectively. The joint openings along the entire crest in massless foundation with 10% damping ratio are still larger than the corresponding results of the viscous-spring boundary model with 5% damping ratio for dam. It appears that a higher damping ratio (say 12-15%) may be necessary for the massless foundation model to obtain comparable results.

The comparison results of the linear elastic and nonlinear analysis are summarized in Table 4.2.

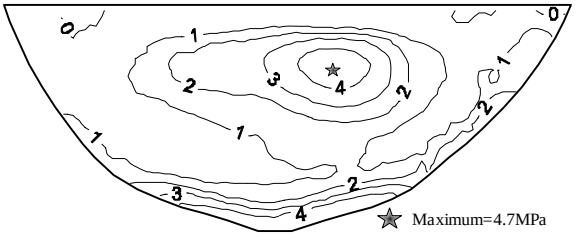

(I) Upstream

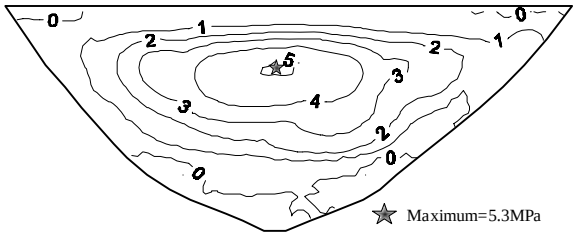

(II) Downstream

(a) Massless foundation input model with 5% damping ratio for dam

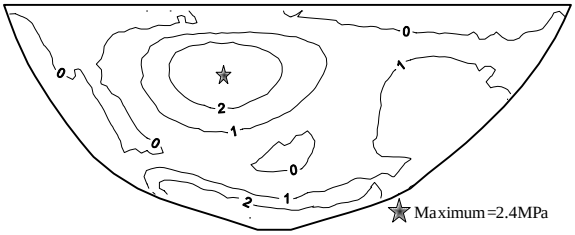

(I) Upstream

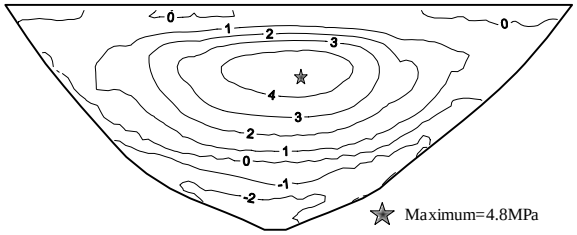

(II) Downstream

(b) Massless foundation input model with 10% damping ratio for dam

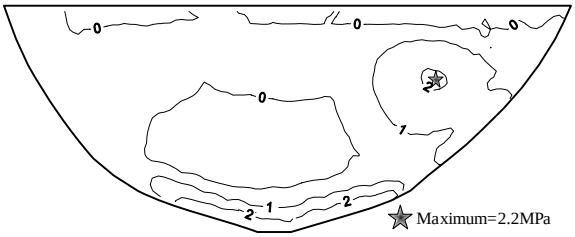

(I) Upstream

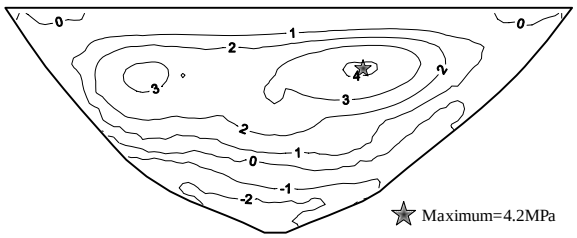

(II) Downstream

(c) Viscous-spring boundary input model with 5% damping ratio for dam

Figure 8 Maximum principal stresses from nonlinear analysis

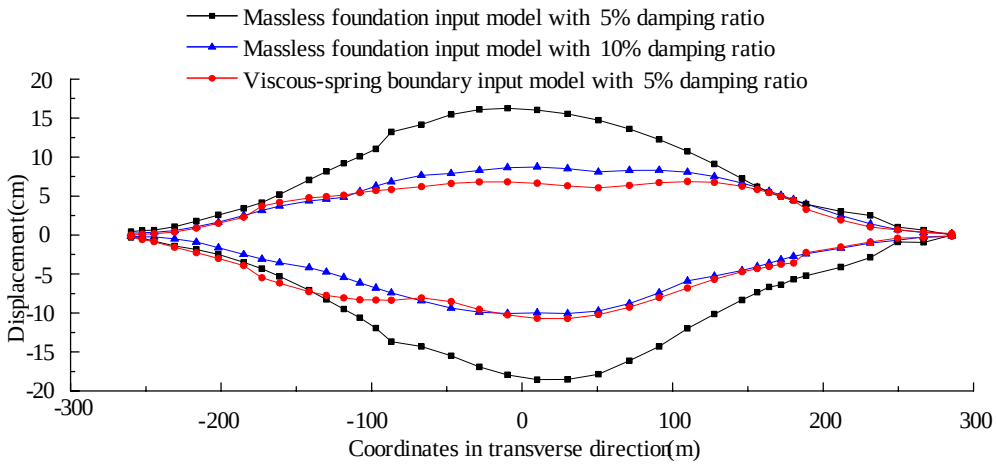

Figure 9 Maximum displacements along the dam crest from nonlinear analysis

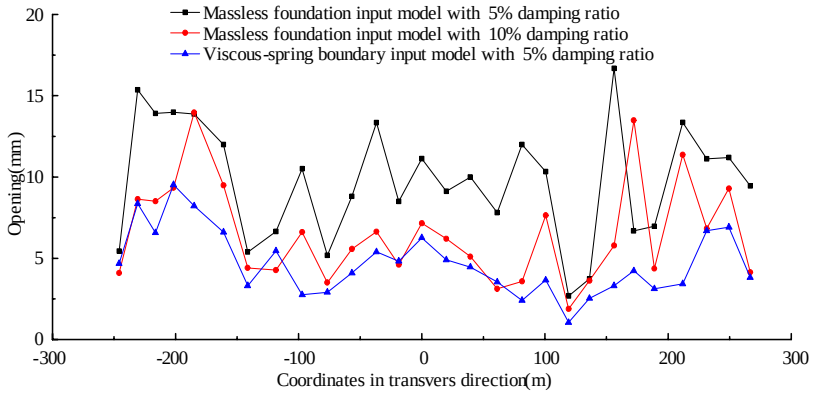

Figure 10 Maximum contraction joint openings from nonlinear analysis

Table 4.2 Maximum values of the analyses

	Cases	Displacement(+) (cm)	Displacement(-) (cm)	Stress (MPa)	Opening (mm)
Linear elastic analysis	Massless foundation input model (5% structural damping)	16.4	-15.8	4.8	—
	Massless foundation input model (10% structural damping)	7.8	-9.6	3.6	—
	Viscous-spring boundary model (5% structural damping)	6.5	-10.3	3.7	—
Nonlinear analysis	Massless foundation input model (5% structural damping)	16.2	-18.5	5.3	16.7
	Massless foundation input model (10% structural damping)	8.7	-10.1	4.8	13.8
	Viscous-spring boundary model (5% structural damping)	7.1	-10.7	4.2	9.6

2.4. Comparison Study on Damage-Cracking of the Dam by Different Foundation Input Models

For studying damage-cracking of the dam, a plastic-damage model developed by Lee and Fenves [33] is used to model stiffness degradation under cyclic loading conditions. Considering tensile cracking is the most common failure phenomenon while the compressive stresses usually have sufficient safety factors in concrete dams, the compressive damage of crushing is not considered herein. The constitutive relations of the plastic-damage model under uniaxial cyclic loading condition is shown in Figure 15 (a), where d_t denotes the damage variable in tension state, hence, $(1\text{-}d_t)E_0$ represents the residual stiffness after degradation; w_t and w_c are respectively weighting factors for controlling the stiffness recovery when loading changes from one state to another. Herein, the tensile strength of concrete is assumed to be 3.25 MPa and other parameters are the same as listed in Table 4.1. For analysis of damage-cracking behavior, the two-third of the dam body is discretized into refined elements with mesh size of about 2 m. The details of modeling may be found elsewhere [57]. The comparison study includes two seismic input models, i.e. massless foundation and viscous-spring boundary model, two assumptions for material modeling, i.e. linear elastic and plastic-damage model; different structural

damping ratios of 0.05, 0.10, 0.15 for massless foundation model and 0.05 for viscous-spring boundary model. Contraction joint opening is considered for all cases of study.

The distribution of damage variables of the dam is shown in Figure 11. It is seen that a region of maximum damage variable d_{max} of 0.9 penetrates through the whole section in the upper portion of the dam when massless foundation is assumed. However, when the viscous-spring boundary is used considering radiation damping, the damage region is limited to a localized area near the down-stream face. The value of d_{max} is also greatly reduced from 0.9 to 0.6. Interestingly, the contours of damage variables obtained from massless foundation model with 10% structural damping ratio are again close to that from viscous-spring boundary model implying a conclusion similar to those obtained in previous sections.

The crest displacements and joint opening are shown in Figures 12 and 13. Several important findings are obtained: (i) In all cases, the damage cracking and massless foundation input model with 5% structural damping ratio gives the maximum response envelopes of displacements with a peak value of 30 cm (Figure 12) and joint openings of 3.5 cm (Figure 13 (a)); (ii) When using the massless foundation input model with 10-15% structural damping ratio, the envelopes of displacements and joint openings are greatly reduced and close to that from viscous-spring boundary model. (iii) Great difference of the displacements and joint openings are obtained between the two material models when massless foundation input model with 5% damping ratio is used (Figure 13 (b)). The reason for that is because, in this case, the serious damage region in the upper portion of the dam causes a significant degradation of structural stiffness; however, by considering the radiation damping effects or by increasing the structural damping ratio to 10-15% for massless foundation, the effects of different material models (linear or damage) on the displacement and joint opening response become much smaller (Figures 13(c) and 13(d)). In this case, the joint openings at the central portion of the dam by the damage model are still larger than that by the linear elastic model, while the joint openings at the quarter or side portion of the dam behave as an opposite tendency due to different capability of load transfer in arch direction between the two material models.

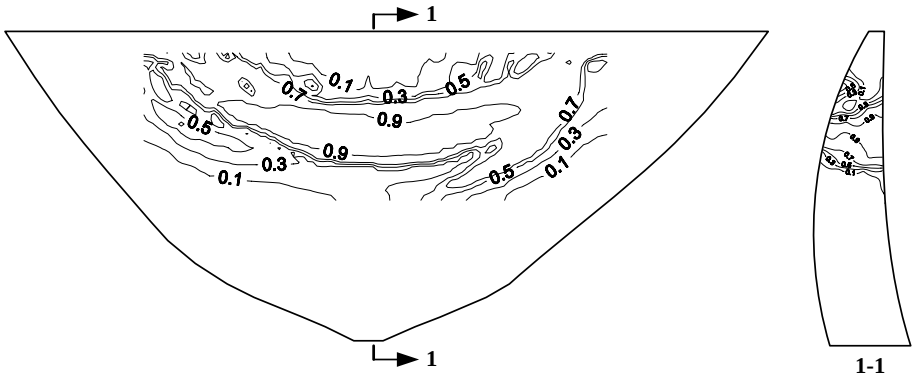

(a) Massless foundation input model with 5% structural damping

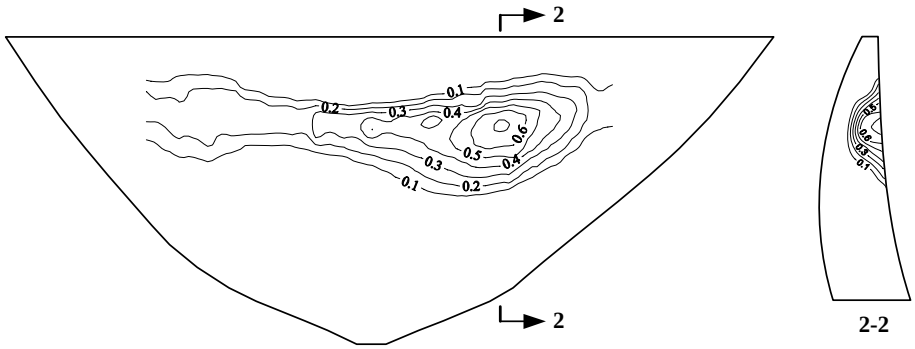

(b) Massless foundation input model with 10% structural damping

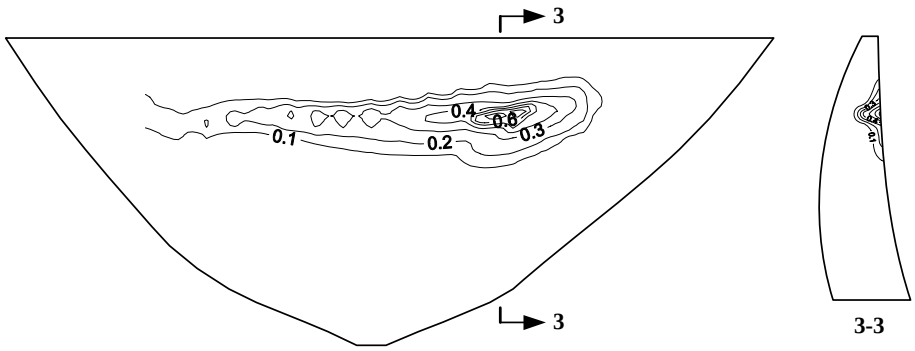

(b) Viscous-spring boundary model with 5% structural damping

Figure 11 Distribution of damage variable *d* on downstream face

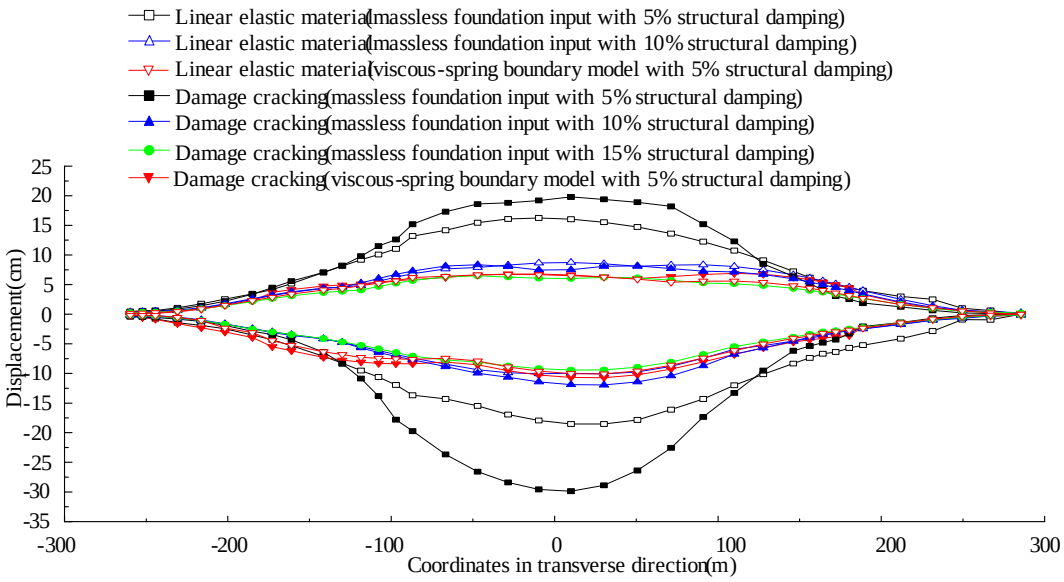

Figure 12 Comparison of maximum displacements at dam crest between different material and input models

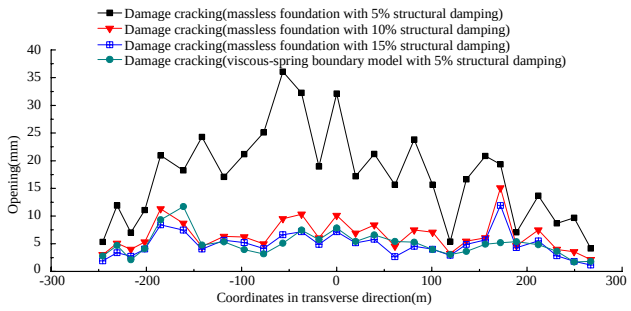

(a) Damage-cracking analysis

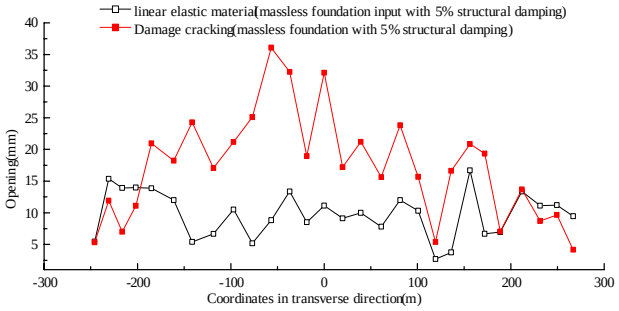

(b) Massless foundation with 5% structural damping

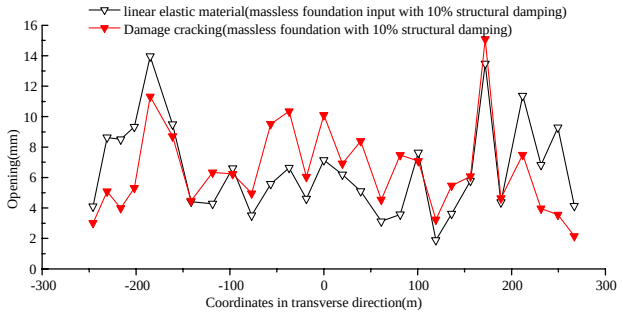

(c) Massless foundation with 10% structural damping

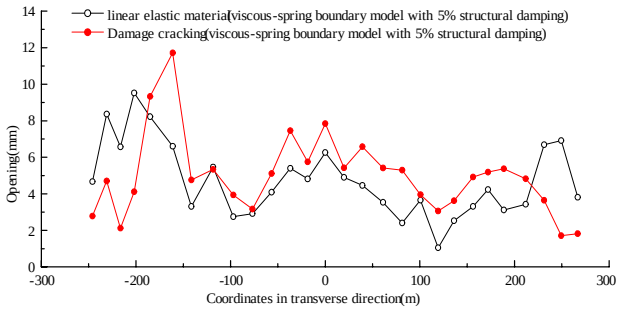

(d) Viscous-spring boundary with 5% structural damping

Figure 13 Comparison of joint opening between different material and input models

2.5. Strengthening of the Dam to Resist the Design Earthquakes

Cantilever reinforcements have been selected as a major strengthening measure for the Dagangshan arch dam. The modeling of the reinforcements in massive concrete in arch dams is briefly introduced in the preceding section and its details may be found elsewhere [58].

The layout of reinforcements is shown in Figure 14, where three layers of reinforcements are equivalently smeared into the membrane elements. The amounts of dam concrete, cantilever steel and arch steel used in the design are 3.14×10^6 m^3, 7210 tons and 2140 tons with a steel-concrete volume ratio of 0.029%. Concrete

properties are the same as listed in Table 4.1. The tensile strength and fracture energy of concrete are f_t=3.25 MPa and G_F=250 N/m respectively. The steel properties are: E_s=260 GPa; v_s=0.3; f_y(yield strength)=650 MPa and 560 MPa for cantilever and arch steel respectively; ρ_s=7800 kg/m3. The constitutive relations of concrete and reinforced steel are show in Figure 15.

The modified embedded-steel model has been implemented in ABAUQS and used in the analysis.

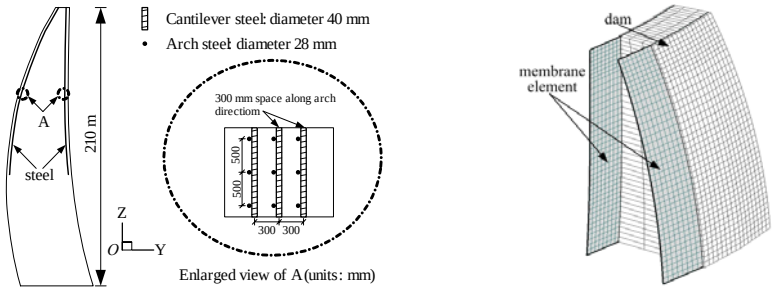

Figure 14 Layout of the strengthening measure with reinforced steel

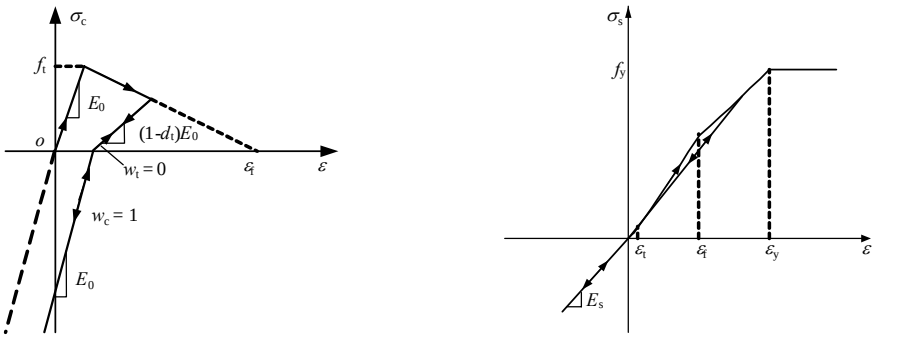

(a) constitutive relation of concrete (b) constitutive relation of steel in cantilever direction

Figure 15 Constitutive stress-strain relations of concrete and reinforced steel

Figure 16 shows the envelopes of contraction joint openings. The maximum opening of joints decreases from 35.6 mm without reinforcement to 28.7 mm with cantilever reinforcement. The openings of joints in the middle region decrease noticeably while those of the other joints near abutments appear little difference.

It is noteworthy that although the peak acceleration of the ground motion beyond 15 s are gradually decreased (not shown), the joint opening occurred in this time range still approaches, if not exceed the maximum opening in the case without reinforcement (Figure 17). This phenomenon shows that even smaller ground motion impulses after the major ones may aggravate the response of the dam and produce a significant residual opening due to damage accumulation. However, the joint openings and displacements obtained with cantilever reinforcement are much lower in this time range (Figures 17 and 18), indicating the reinforcements carry considerable tensile loads transferred from cracked concrete and prevents the cracks from penetrating the whole section of the dam.

In addition, the equilibrium lines of these oscillating displacement histories shifts toward upstream direction in both analyses (Figure 18), which are caused by the accumulations of tensile plastic strain after cracking. This phenomenon indicates that there will be a remarkable residual deformation toward the upstream direction after the earthquake.

The evolution of concrete cracking at the downstream face is shown in Figure 19, where the cracking strain

e_{cr} denotes the maximum cracking deformation occurred during the earthquake. The evolution process in these two analyses shows the difference at all instances listed in the figure; the cracking strain values obtained with cantilever reinforcement are smaller than those obtained without strengthening. The results from Figure 20(a) indicate that the concrete cracks will penetrate the monoliths if reinforcements are not used.

The cracking evolution of monolith at x = -56 m is shown in Figure 20. The results show that concrete damage in these two analyses occurs in the downstream zone at the same instance and extends to the upstream face with similar evolution behavior. The results also show cantilever reinforcement significantly limits the extension of concrete crack and prevents the monolith from penetration of entire cross section. Moreover, the maximum value of cracking strain decreases from 3.6×10^{-3} to 2.4×10^{-3} (a decrease of 33.3%).

All the aforementioned results show that cantilever reinforcements can not prevent the dam from cracking because of its low ratio of reinforcement. However, the reinforced steel can carry considerable tensile load transferred from the cracked concrete and improve the stiffness of monolith after concrete damage occurs in the dam. Therefore, the reinforced steel has effects on decreasing the responses of joint opening and displacements as well as limiting crack extension. In addition, the accumulation of tensile plastic strain caused by the concrete damage occurred in the downstream zone may cause residual deformation toward upstream direction. This is even more severe in the case without cantilever reinforcement, which may weaken the load-carrying capacity of the dam.

Consequently, the strengthening measure of cantilever reinforcement has a noticeable benefit for improving earthquake-resistant capacity of the Dagangshan arch dam. Moreover, this study shows that the modified embedded-steel model is applicable to evaluating the effectiveness of reinforcement strengthening and optimizing the design of strengthening measures.

However, the effect of current reinforcement measure is not sufficient to reduce the damage-cracking development of the dam. Therefore, extensive studies of being conducted to investigate the effect of combining seismic-resistant measures are cantilever reinforcement with other strengthening methods, including joint dampers. Moreover, the influence of canyon radiation may be considered in the further investigation.

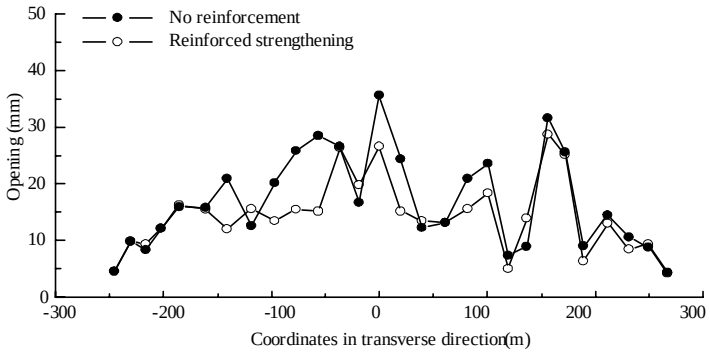

Figure 16 Envelope of joint opening

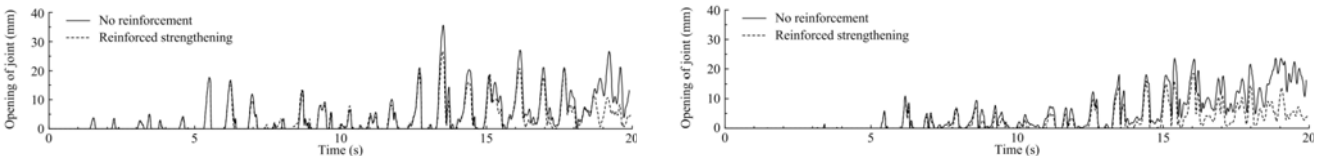

(a) x=0 m (b) x=100 m

Figure 17 Time histories of joint opening at x=0 and 100 m

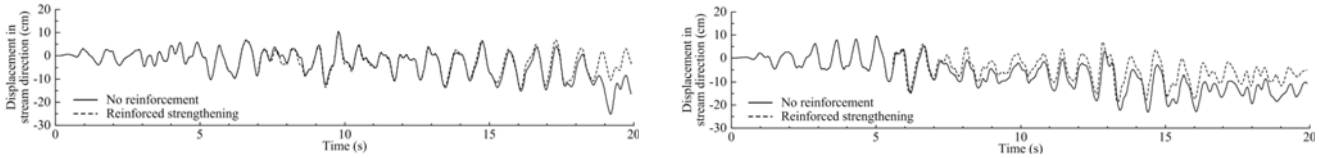

(a) x=-97 m (b) x=100 m

Figure 18 Displacement histories of crest nodes in stream direction at x=-97 and 100 m

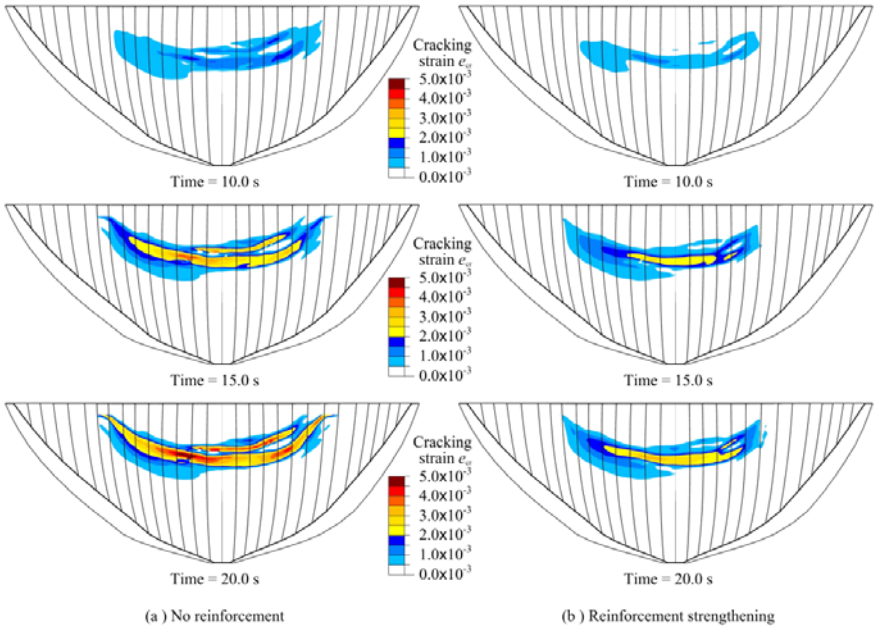

Figure 19 Evolution of cracking strain e_{cr} at the downstream face (without reinforcement)

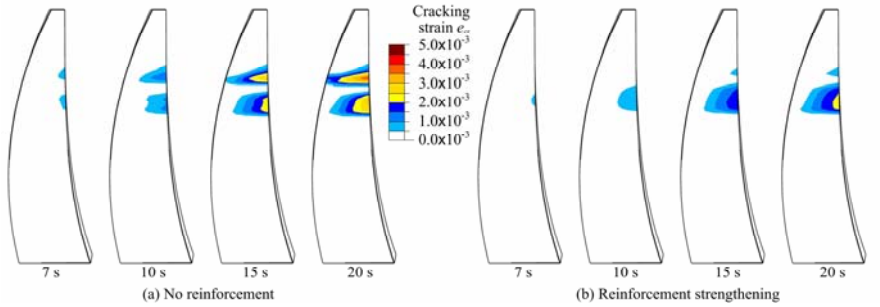

Figure 20 Evolution of cracking of the monolith at x = -56 m

3. Concluding Remarks

(1) Several key issues regarding seismic safety evaluation of high concrete dams, especially arch dams have been studied. Among those, the earthquake input mechanism and foundation modeling may be one of the most important issues in this regard. It is found that compared with the conventional massless foundation model and uniform input of ground motion, the radiation damping and non-uniform motions due to infinite canyon have important effects leading to a 25-40% reduction in dam response. Equivalently, use of a larger damping ratio for

structures such as 10-15% may also obtain comparable results of dam response to that of considering radiation damping. This benefit may be (at least partially) considered in the design or as a potential safety factor for resisting strong earthquakes;

(2) Contraction joint opening is another important factor needed to be considered in safety evaluation. The main concern of this nonlinearity is the maintenance of integrity of the dam body and prevention of water stops between joints from breakage. Studies from several arch dams of 200-300 meters in height including Xiaowan, Xiluodu and Dagangshan Dams reveal that the maximum joint openings are in the level of 10-15 mm when the linear elastic model of concrete material is applied, or 20-35 mm when damage-cracking model for concrete is used. With a special design for withstanding 50-80 mm in deformation for water stops, the influence of such opening to safety of water stops can be manageable.

(3) Tensile stresses in cantilevers will remarkably be increased due to the response amplification of the dam and joint opening. Thus, damage-cracking will inevitably occur in the upper middle portion of the dam. In the massless foundation analysis for the Dagangshan case, a serious damage area with degradation index of 0.9 is observed from downstream to upstream faces for most of the middle cantilevers, indicating the cracks may penetrate the whole section of the most middle cantilevers. However, when the radiation damping of the infinite canyon is considered, the damage-cracking area will be significantly reduced to a localized downstream region and the maximum degradation index is also decreased to 0.6. Nevertheless, for retaining a sufficient safety margin in the design, it was decided to adopt strengthening measures of cantilever reinforcements and joint dampers in the Dagangshan and Xiaowan arch dams. It is hoped that the predicted earthquake behavior of high arch dams and the effectiveness of strengthening measures can be further verified.

(4) Other important issues such as arch dam-reservoir interaction and dynamic dam-foundation stability are only briefly touched in Part I of the paper. They also need further investigation in the future.

(5) Although more advanced knowledge and sophisticated numerical methods for earthquake analysis of large concrete dams appear to be available to date, realistic earthquake behavior and damage mechanisms of large dams are still far from states of complete clarity. The conventional seismic design practice is that the pseudo-static arch-cantilever method is still used for dam design and the rigid body limit equilibrium for foundation. However, when earthquake input mechanisms and nonlinear interaction behaviors of the system are involved, how to link up the interpretations from these two categories of methods is a crucial issue in safety evaluation of large dams.

ACKNOWLEDGEMENTS

The authors gratefully acknowledge financial support for this work provided by the National Natural Science Foundation of China: 90510018 and 90715041; the National Basic Research Program: 2002CB412709; and Chengdu Hydroelectric investigation & Design Institute. Appreciation is also expressed to Professor Wang Guanglun, Dr. Xu Yanjie and Dr. Wang Jinting for their valuable discussion in communication during the research.